ACS Catalysis

pubs.acs.org/acscatalysis

Research Article

Hydrolysis of Acetamide on Low-Index CeO_2 Surfaces: Ceria as a Deamidation and General De-esterification Catalyst

Suman Bhasker-Ranganath and Ye Xu*

Cite This: *ACS Catal.* 2022, 12, 10222−10234

Read Online

ACCESS | Metrics & More | Article Recommendations | Supporting Information

ABSTRACT: Using DFT calculations and acetamide as the main example, we show that ceria is a potential catalyst for the hydrolysis of amide and similar bonds. The overall reaction is endergonic in the gas phase, yielding acetic acid and ammonia, but is slightly exergonic in the aqueous phase, which facilitates ionization of the products (CH_3COO^- and NH_4^+). Neighboring Ce and O sites on the CeO_2(111), (110), and (100) facets are conducive to the formation of an activated metastable tetrahedral intermediate (TI) complex, followed by C−N bond scission. With van der Waals and solvation effects taken into account, the overall reaction energetics is found to be most favorable on the (111) facet as desorption of acetic acid is much more uphill energetically on (110) and (100). We further suggest that the Ce−O−Ce sites on ceria surfaces can activate X(=Y)−Z type bonds in amides, amidines, and carboxylate and phosphate esters, among many others that we term "generalized esters". A Brønsted-Evans−Polanyi relationship is identified correlating the stability of the transition and final states of the X−Z generalized ester bond scission. A simple descriptor ($\Sigma\Delta\chi$) based on the electronegativity of the atoms that constitute the bond (X, Y, Z) versus those of the catalytic site (O, Ce, Ce) captures the trend in the stability of the transition state of generalized ester bond scission and suggests a direction for modifying ceria for targeting specific organic substrates.

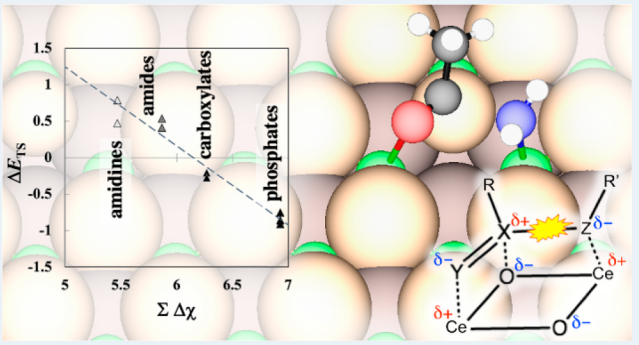

KEYWORDS: *deamidation, de-esterification, hydrolysis, generalized ester, enzyme mimic, ceria, density functional theory, descriptor*

1. INTRODUCTION

The stability of peptides, proteins, antibodies, and some polymers is largely attributed to their amide (C(=O)−N) bonds, which retain a partial double bond character via resonance stabilization.[1] Large rotational barriers associated with the amide C−N bonds help preserve the 3D structure of amino acid chains in proteins.[2] Scission of peptide bonds in peptides and proteins (deamidation), and of C−N bonds in related C(=X)−N compounds, such as amidines, plays a fundamental role in proteomics, therapeutics, chemical genetics, analytical biochemistry, and biotechnology. In environmental and biochemical settings, the reaction proceeds through the formation of a tetrahedral intermediate (TI) following nucleophilic attack at the carbonyl C by water.[3,4] A base-catalyzed mechanism, in which a hydroxide group functions as the nucleophile, appears to be operative even in neutral aqueous solutions.[5−7] Oxygen exchange between amides and water is observed, which is attributed to reversible formation of the TI. The dissociation of the C−N bond in the TI is the rate-limiting step, in contrast to the dissociation of the C−O bond in the hydrolysis of carboxylate esters where the formation of the TI is rate-limiting because alkoxides (−OR) are better leaving groups than amides ($-NR_2$).[4,8] At neutral pH and ambient temperature, peptide bonds have a long half-life of 250−600 years, with respect to nonenzymatic hydrolysis.[9,10]

Enzymes such as peptidase and deaminase catalyze the hydrolysis of amide C−N bonds in a narrow range of pH and temperature. Many peptidases do not contain metals, while a particular subclass, metallopeptidase, does use metal cations to catalyze the reaction. Representative members of this class include carboxypeptidase A and thermolysin, both of which contain a Zn^{2+} at their active sites. How Zn^{2+} accelerates amide C−N bond scission has long been debated.[11−13] The role of Zn^{2+} is currently understood as positioning the carbonyl group by coordinating to its O atom, stabilizing a water molecule or hydroxide group that attacks the carbonyl C, and stabilizing one or both negatively charged C−O groups.[13,14] There is also evidence that intramolecular nucleophilic attack by an hydroxyl or thiol group that is a part of certain amino acids (e.g., serine, threonine, and cysteine) on the central C helps break the

Received: May 23, 2022
Revised: July 12, 2022
Published: August 5, 2022

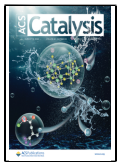

https://doi.org/10.1021/acscatal.2c02514
ACS Catal. 2022, 12, 10222−10234

amide C−N bond under unfavorable external pH conditions, which is referred to as N−O/S acyl rearrangement.[15,16]

Interest in artificial metallopeptidase has been growing.[14,17,18] Based on the understanding of the action of metallopeptidase, complexes of Cu^{2+},[19,20] Pd^{2+},[21] Pt^{2+},[22] and Co^{3+} (ref 23) have been investigated for catalytic hydrolysis of amides and peptides under mild conditions. Kita et al. reported Zn acetate and Zn triflate to have higher deamidation activity than Co, Mn, and Cu acetates, while Pd, Ni, and Ag acetates have no activity.[24] Even the inorganic salt $ZnCl_2$ has noticeable deamidation activity, but Zn dust, which is likely oxidized Zn, has little activity.[24,25] Alcohols can be used in lieu of water for the alcoholysis of amides.[24]

Solid heterogeneous catalysts have certain advantages over homogeneous catalysts with respect to recovery and separation from reaction media. Since the first reports in 1950s,[26,27] complexes of Ce^{4+} have been investigated for catalyzing the hydrolysis of small peptides[28,29] and proteins[30−33] in homogeneous solutions. Higher conversions were reported for Ce^{4+} complexes than Ce^{3+} and other metal ion species, which is attributed to the large coordination number of Ce^{4+} and its ability to form a more stable reduced Ce^{3+} state by withdrawing electrons from the amide linkage. This has led to investigation into solid ceria (CeO_2) as a possible deamidation catalyst. Over the past decade, Shimizu and co-workers demonstrated efficient alcoholysis and subsequent esterification of amides over high loadings of CeO_2 in batch mode in hot, boiling alcohols.[34−37] Recently, the same group investigated the hydrolysis of acetamide under similar conditions of boiling solvents and high catalyst loadings using various solid oxides including Nb_2O_5, ZrO_2, CeO_2, TiO_2, SiO_2, and Al_2O_3, among others as catalysts.[38] The first three oxides were reported to achieve conversion of acetamide to acetic acid over 45%, including 100% conversion over Nb_2O_5. The authors proposed mechanisms for the hydrolysis and alcoholysis of amides based on the concerted actions of Lewis-acidic metal cation and basic O anion that attack the carbonyl O and carbonyl C, respectively, and supported them with density functional theory (DFT) calculations on CeO_2(111).[35,38] They also identified a correlation between the increasing basicity of lattice oxygen in metal oxides, as represented by the O_{1s} binding energy, and higher initial reaction rates for several oxides. It remains unclear why CeO_2 is more effective than Nb_2O_5 in alcoholysis[37] but not in hydrolysis.[38]

Ceria-catalyzed hydrolysis and alcoholysis reported thus far in the literature have been based on commercially available polycrystalline ceria powder.[34−38] It is not clear which low-index facet or what surface structure, if any, plays a dominant role in the observed deamidation activity. Surface structure sensitivity has been observed for many reactions on ceria.[39−42] Mullins and co-workers showed that small organic molecules, including water, alcohols, acetic acid, and acetaldehyde, exhibit qualitatively different temperature-programmed desorption (TPD) results on CeO_2(111) vs CeO_2(100) thin films.[43] Ceria nanocubes and nanorods, which predominantly expose (100) and/or (110) facets, and nano-octahedra, which predominantly expose (111) facets, exhibit different activities or product distributions when catalyzing a wide range of reactions including CO oxidation,[44] ethanol oxidation,[45] carbamoylation,[46] CO_2−methanol coupling,[47] and aqueous-phase dephosphorylation.[48] The differences are variously attributed to factors including different binding strength, basicity of lattice oxygen, and reducibility of the facets.[49,50]

In the present work, we perform periodic DFT calculations to examine in detail the mechanism of hydrolysis of the amide C−N bond, using acetamide as the main model compound, on the three low-index facets of CeO_2: (111), (110), and (100). The basic reaction pathway, as will be presented and discussed below, is outlined in Figure 1. Because of the significance of deamidation reactions in biochemical contexts, the effects of solvation and dispersion interactions are taken into consideration using an implicit solvation model and a van der Waals functional, respectively. We further consider C−N bond scission in benzamide, *N*-methylacetamide, acetamidine, and adenine on CeO_2(111) to highlight the ability of the Ce−O−Ce site ensemble to adsorb and activate C(=X)−N bonds, which is representative of the reactivity of ceria toward an even broader class of heteroatomic organic compounds containing the motif of X(=Y)−Z, including organic amides, phosphates, and carboxylates, all of which we term generalized esters (GEs). Our results shed light on the fundamental properties that endow ceria with versatile reactivity toward biologically and environmentally relevant organic molecules, including peptides and nucleobases. They make ceria a promising enzyme-mimetic material for the development of novel diagnostic, pharmaceutical, and therapeutic technologies, among others.[51−53] The main challenge for ambient temperature hydrolysis applications is identified to be the desorption of the carboxylate product.

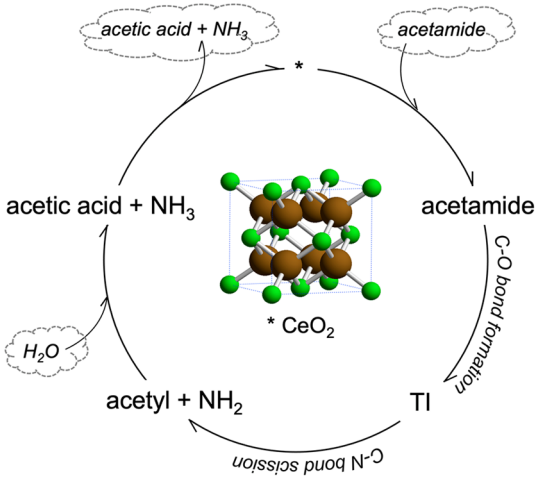

Figure 1. Schematic illustrating the overall reaction pathway for acetamide deamidation and hydrolysis on ceria. Asterisk symbol (*) denotes catalytic sites. TI stands for tetrahedral intermediate. Species in cloud are located off the catalyst.

2. METHODS

Periodic DFT calculations were performed within the generalized gradient approximation (GGA-PW91[54]) and with van der Waals corrections (optB86b-vdW),[55−58] using the Vienna Ab initio Simulation Package (VASP)[59−62] and Quantum Espresso (QE).[63,64] The potentials due to core electrons were described using the projector-augmented wave (PAW) method,[65,66] and the Kohn−Sham valence states were expanded in a plane wave basis set with a cutoff energy of 400 eV in VASP. PAW potentials for Ce, O, and C, and ultrasoft pseudopotentials (USPP) for H and N, all taken from the standard solid-state pseudopotentials (SSSP) library v1.1.2,[67] were used in QE.

https://doi.org/10.1021/acscatal.2c02514
ACS Catal. 2022, 12, 10222−10234

The (111), (110), and (100) facets of CeO_2 were modeled as p(3 × 3) slabs (Figure 2) of 9, 4, and 9 atomic layers

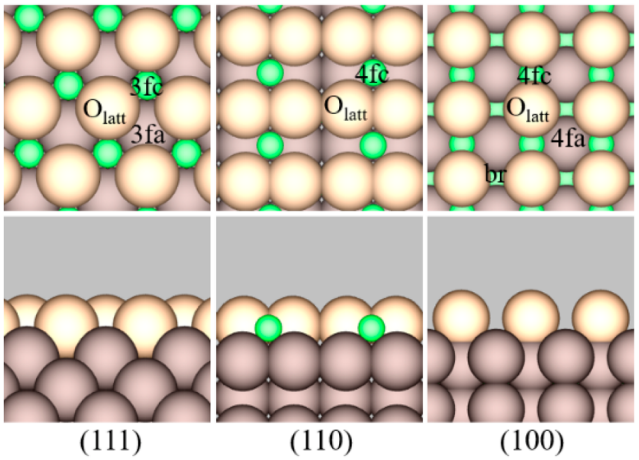

Figure 2. Top (top panels) and side (bottom panels) views of the respective low-index stoichiometric CeO_2 facets, with the surface sites labeled. [Color code: green, Ce; light brown, surface O_{latt}; and dark brown, subsurface O_{latt}. Site designations: 3fa, 3fc, 4fa, 4fc, and br refer to the 3-fold anion, 3-fold cation, 4-fold anion, 4-fold cation, and bridge sites, respectively.]

(corresponding to 3, 4, and 4 O−Ce−O trilayers), with periodic images of the slabs separated by 12−16 Å of vacuum and dipole decoupling applied in the z-direction. A Γ-centered Monkhorst−Pack 2 × 2 × 1 k-point grid was used to sample the surface Brillouin zone.[68] Adsorption of a single molecule per surface unit cell resulted in 1/9 monolayer (ML) coverage. The top three, two, and five atomic layers of the (111), (110), and (100) slabs were relaxed, respectively, while the remainder of each slab was held fixed at bulk coordinates. Oxygen vacancies were not considered, because those in the surface and near-surface regions are readily blocked or annihilated by the oxygenate species involved in this reaction system such as water and acetate,[69−71] and more generally, by O_2 and water occupying and dissociating in them in ambient settings. Geometry optimization was performed until the maximum residual force was 0.03 eV/Å or less in each relaxed degree of freedom.

The adsorption energy (ΔE_{ads}) was evaluated as $\Delta E_{ads} = E_{total} - E_{slab} - E_{gas}$, where E_{total}, E_{slab}, and E_{gas} refer to the total energies of a slab with an adsorbate, the slab without any adsorbate, and the isolated adsorbate in gas phase, respectively. A more negative value of ΔE_{ads} indicates stronger bonding between an adsorbate and a slab. Gas-phase species were optimized in a $(15\ Å)^3$ simulation cell, with dipole decoupling applied in all directions in VASP[72] and with the Martyna−Tuckerman correction applied in QE.[73]

The elementary steps with associated transition states (TS) in the catalytic C−N bond scission and hydrolysis of acetamide and other GEs were determined using the climbing-image nudged elastic band method[74,75] and dimer method[76,77] until the maximum residual force converged to 0.03 eV/Å or less in all relaxed degrees of freedom. The reaction energy (ΔE_{rxn}) was evaluated as $\Delta E_{rxn} = E_{FS} - E_{IS}$, and the activation barrier (E_a) was evaluated as $E_a = E_{TS} - E_{IS}$, where E_{IS}, E_{TS}, and E_{FS} are the total energies of the initial, transition, and final states, respectively. Each TS was verified to possess only one vibrational mode with a negative curvature in the direction of the reaction under consideration. Vibrational modes and frequencies were calculated using finite difference approximation of the dynamical matrix with a displacement of 0.01 Å. Infrared spectra of adsorbed states were simulated using Atomic Simulation Environment (ASE).[78]

The DFT+U approach of Dudarev et al.[79] was employed to partially rectify the delocalization of Ce 4f states resulting from self-interaction error.[50] A U_{eff} value of 2 eV was used in this study based on better agreements between GGA+U predictions obtained at U_{eff} = 2−3 eV and available experimental measurements, including the bulk reduction energy of CeO_2,[80,81] chemisorption energy of CO on CeO_2(110),[82] and peak desorption temperatures of AcH.[83] The calculated equilibrium lattice constants of 5.476 Å (GGA-PW91) and 5.452 Å (optB86b-vdW)[84] are in good agreement with the experimental value of 5.41 Å.[85,86]

The effects of solvation by water were modeled implicitly by treating the solvent as a dielectric continuum. While VASPsol[87,88] has been popularly used to study solvation effects for a variety of molecules and extended structures, self-consistent field (SCF) cycles failed to converge for the CeO_2 facets. Indeed, there has been no study reporting the application of VASPsol to modeling solvation of CeO_2 surfaces, to the best of our knowledge. Therefore, VASPsol was applied only to isolated molecular species at default settings. For periodic CeO_2 slabs, we used the self-consistent continuum solvation (SCCS) model as implemented in Environ for QE,[89,90] with permittivity set to 78.3 and surface tension and pressure both set to 0. A higher cutoff energy of 35 Ry, or 476 eV, was used to improve SCF convergence. While the maximum residual forces converged to below 0.04 eV/Å for molecules, ions, and the clean CeO_2 slabs, they could not be reduced to below 0.3, 0.1, and 0.1 eV/Å for some of the proposed reaction intermediates adsorbed on the (111), (110), and (100) slabs, respectively.

3. RESULTS AND DISCUSSION

3.1. Adsorption of Acetamide. Two stable molecular adsorption configurations can be found for acetamide on the stoichiometric CeO_2 facets: the η^1 state (Figures 3a−c), in which acetamide is located above a 3fc or 4fc site through C═O with one of the amine H atoms simultaneously interacting with a neighboring O atom in the oxide surface (denoted O_{latt}; see Figure 2); and a metastable state, in which acetamide binds to an O_{latt} through its central carbonyl C, with the carbonyl O and the amine N each coordinated to an adjacent Ce (Figures 3d−f). Strong Lewis acid−base interaction between the Ce cation and the carbonyl oxygen of acetamide is previously concluded by Kamachi et al.[35] Key bond distances in the minimum-energy structures shown in Figure 3 are reported in Table 1.

Adsorption in the η^1 state causes minimal changes in the geometry of acetamide, which appears to be a nonactivated process. The η^1 state, because of its polarized C═O and C−N bonds, is open to nucleophilic attack on the central C by a nucleophile, e.g., O_{latt} in the surface. It must overcome an activation barrier as the sp^2 hybridization of the >C═O group transitions to sp^3 hybridization that is seen in the TI in the hydrolysis of amide and peptide bonds by biochemists.[4,7,11,23,91,92] In metal ion-catalyzed hydrolysis, binding of the carbonyl O to a metal ion, followed by nucleophilic attack by water or OH, results in the formation of the TI complex. In contrast, here the TI is formed directly on CeO_2 surfaces

https://doi.org/10.1021/acscatal.2c02514
ACS Catal. 2022, 12, 10222−10234

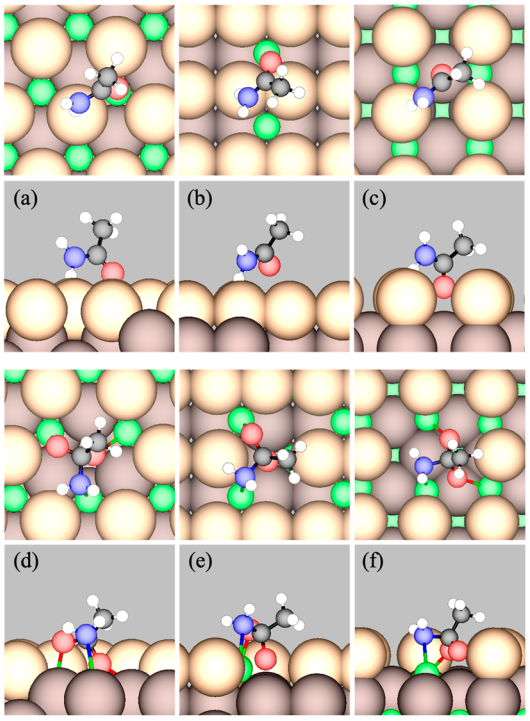

Figure 3. Top (top panels) and side (bottom panels) views of GGA-PW91 optimized acetamide adsorbed in the (a–c) η^1 and (d–f) TI state on the left, (111); middle, (110); and right, (100) facets of CeO_2 respectively. [Color code: green, Ce; light brown, surface O_{latt}; dark brown, subsurface O_{latt}; red, O in molecule and O_{latt} directly bonded to C; black, C; blue, N; and white, H.]

without an additional nucleophile due to the presence of adjacent acid–base sites. The calculated E_a values for this conversion (step b → c, Table 2) are 0.65, 0.57, and 0.80 eV on the (111), (110), and (100) facets, respectively. For comparison, Kamachi et al. calculated this E_a value to be 0.73 eV for acetamide on (111) using GGA-PBE and an atomic basis set.[35] Similar complexes have been previously predicted theoretically for dimethylcarbonate,[46,93] benzyl acetate,[35] and phosphate monoesters on CeO_2(111).[94,95] The C═O and C–N bonds lengthen significantly from the η^1 state to the TI state (Table 1), suggesting the latter to be a precursor state to the dissociation of the C–N bond.

The adsorption energies (ΔE_{ads}) of the molecular species adsorbed on the three CeO_2 facets in this reaction calculated using GGA-PW91 and optB86b-vdW are listed in Table S1 in the Supporting Information, together with available literature values. ΔE_{ads} consistently follows the trend (111) > (110) > (100) (i.e., adsorption most stable on (100)), according to both GGA-PW91 and optB86b-vdW, including acetamide in the η^1 and TI states. The trend reflects the fact that the combined local coordination of the topmost Ce and O_{latt} atoms is the lowest on (100) and highest on (111).[96] Stronger binding of the products (acetic acid and NH_3) than the reactants is evident.

Kamachi et al. reported Fourier transform infrared (FTIR) spectra of gas-phase acetamide exposed to polycrystalline CeO_2 at 120 °C.[35] Three prominent peaks were found at 1430, 1554, and 1656 cm^{-1}. The 1656 cm^{-1} peak was attributed to the ν(C═O) mode of η^1 acetamide, the intensity of which decreased appreciably on the order of minutes. This assignment agrees with our simulated IR spectra for acetamide (see Figure S1 in the Supporting Information), which put this mode at 1620–1640 cm^{-1} on the three lowest-index facets of ceria. The mode is absent in the TI, nor is IR detection of it expected, because of the metastable nature of the TI and facile C–N bond scission (see the next section). The other two peaks in the FTIR increased in intensity with time and were attributed to acetate species. The peaks at 1430 and 1554 cm^{-1} agree with previous IR studies of acetic acid adsorbed on CeO_2(111)[71] and polycrystalline ceria.[97,98] They are consistent with our analysis below, which suggests acetate to be desorption-limited.

3.2. Deamidation and Hydrolysis of Acetamide. Based on the literature, we propose and investigate the following mechanism for the deamidation and hydrolysis of acetamide, which represents a direct reaction pathway to the products, acetic acid and ammonia. The steps include (1) adsorption of acetamide in the η^1 state and then the TI; (2) C–N scission forming acetyl and NH_2; (3) adsorption of H_2O; (4) hydrogenation of NH_2 forming NH_3; (5) attack of acetyl by OH forming acetate; (6) desorption of NH_3 and acetic acid. The reaction parameters for each of these steps on the three low-index CeO_2 facets calculated using GGA-PW91 are tabulated in Table 2. The snapshots of the intermediate states on the (111) facet are shown in Figure 4, and those on the (110) and (100) facets are shown in Figures S2 and S3, respectively, in the Supporting Information. The minimum-energy reaction energy profiles based on the intermediate states and elementary steps proposed in Table 2 are mapped out in Figure 5. Since free-energy contributions at the gas/solid

Table 1. GGA-PW91 Adsorption Energy (ΔE_{ads}) and Key Bonding Distances of Acetamide Adsorbed in the η^1 and TI States, and Activation Barrier for Converting η^1 into TI (E_a) on the Three Low-Index Facets of CeO_2

				Bond Distances (Å)				
state	facet	ΔE_{ads} (eV)	E_a (eV)	C–O_{latt}	N–Ce	O–Ce	C–N	C═O
gas phase	–	–	–	–	–	–	1.37	1.23
η^1	(111)	−0.64	0.65	–	–	2.56	1.34	1.25
	(110)	−0.88	0.57	–	–	2.56	1.34	1.25
	(100)	−1.36	0.80	–	–	2.53/2.54[a]	1.32	1.28
TI	(111)	−0.32		1.45	2.71	2.28	1.50	1.36
	(110)	−0.74		1.43	2.62	2.26	1.53	1.38
	(100)	−1.40		1.41	2.74	2.33/2.67[a]	1.52	1.40

[a]O–Ce bond distances are between ═O and the two Ce constituting the bridge site.

https://doi.org/10.1021/acscatal.2c02514
ACS Catal. 2022, 12, 10222–10234

Table 2. GGA-PW91 Activation Barrier (E_a) and Reaction Energy (ΔE_{rxn}) for the Proposed Elementary Steps in Deamidation and Hydrolysis of Acetamide on the Three Low-Index CeO_2 Facets

		(111)		(110)		(100)	
label	elementary step[a]	E_a (eV)	ΔE_{rxn} (eV)	E_a (eV)	ΔE_{rxn} (eV)	E_a (eV)	ΔE_{rxn} (eV)
a → b	AcD(g) → η^1-AcD	0[b]	−0.64	0[b]	−0.88	0[b]	−1.36
b → c	η^1-AcD → TI	0.65	+0.32	0.57	+0.14	0.80	−0.04
c → d	TI → Ac + NH_2	0.73	+0.62	0.42	+0.19	0.52	−0.25
e → f	H_2O(g) → H_2O	−[b]	−0.53	−[b]	−0.78	−[b]	−0.95
f → g	H_2O → OH + H	0.11	+0.02	0.38	−0.22	0.02	−0.64
c + f → h	TI + H_2O → Ac + NH_3 + OH	0.65	−0.20	–	–	–	–
c + g → d + g	TI + OH + H → Ac + NH_2 + OH + H	0.84	+0.82	0.46	+0.19	0.47	−0.36
d + g → h	Ac + NH_2 + OH + H → Ac + NH_3 + OH	−[c]	–	0.30	−0.76	0.36	−0.07
i → j	NH_3 → NH_3(g)	0.74[b]	+0.74	0.76[b]	+0.76	1.09[b]	+1.09
k → l	Ac + OH → acetate + H	0.17	−0.42	0.23	−0.14	0.78	+0.67
l → m	acetate + H → AcA(g)	0.93[b]	+0.93	1.51[b]	+1.51	1.70[b]	+1.70

[a]AcD = acetamide; Ac = acetyl; AcA = acetic acid. [b]Adsorption is assumed to be barrier-less and desorption is assumed to have no kinetic barrier in addition to a thermodynamic barrier. [c]OH and H recombine to form water before hydrogen transfer to NH_2.

interface are expected to be minor for reactions of small organic compounds on ceria under ambient conditions,[84] they are omitted from Figure 5.

A comparison of the calculated reaction energy profiles for the same overall reaction in gas phase, $AcD_{(g)} + H_2O_{(g)} \rightarrow NH_{3(g)} + CH_3COOH_{(g)}$ (black lines, Figures 5a−c), reveals a progressively deepening energy landscape from (111) to (110) and to (100). The most stable state on each facet is either h (acetyl + NH_3 + OH) or i, l (NH_3, acetate + H), meaning that the reaction is limited by product desorption, at least in the gas phase.

The E_a value for C−N bond scission in the TI (step c → d) producing acetyl and NH_2 is 0.73 eV on (111), and less on (100) and (110). The TS of C−N scission is higher in energy than gas-phase acetamide (i.e., zero on ΔE axis) on (111), meaning that it is more likely for the molecule to desorb than to undergo decomposition on this facet, according to GGA-PW91. The step is endothermic by +0.62 eV on (111) but mildly exothermic on (100) (−0.25 eV). The C−N distance at the TS is 2.25 Å on (111) (Figure 4c‡d), 2.14 Å on (110) (Figure S2c‡d), and 2.06 Å on (100) (Figure S3c‡d). The resulting acetyl group binds to O_{latt} via its carbonyl C. Different from the mononuclear Zn^{2+} active center in CPA and thermolysin,[13,14] the (110) and (111) facets (cf. Figure 2) each provide a pair of Ce^{4+} cation sites at a suitable distance and angle with respect to O_{latt} (the nucleophile attacking the carbonyl C) that can coordinate to both the O and N atoms in acetamide simultaneously in the TS. A parallel situation is found in ester decomposition on metal surfaces, where a triangular ensemble of three metal atoms activates the C(=O)−O bond.[99]

The situation is different on the (100) facet where Ce^{4+} and O_{latt} atoms are linearly aligned, so that in the TI and TS of C−N bond scission, the entire dioxo complex must shift to a nearest br site to better accommodate the rigid O−C−N angle (see Figures S3c and S3c‡d). A much larger barrier exists for the TI to enolize at its methyl end (1.60 eV on (111)), so that reaction pathway is not considered further.

Akin to what has been reported for coadsorbed pairs of open-shell molecules on oxides that have large band gaps,[100−102] cooperative interaction is notable between the molecular fragments produced from C−N bond scission, acetyl, and NH_2, on all three facets, being −0.88, −1.26, and −1.27 eV on the (111), (110), and (100) facets (see Table S2 in the Supporting Information). Therefore, the two fragments are expected to remain in close vicinity of each other at mild temperatures, and NH_2 hydrogenation to NH_3 is investigated in the presence of acetyl.

In agreement with previous reports,[103−105] we find water dissociation by itself to have small barriers on all three facets (Table 2, step e → f). On (111), coadsorption with water lowers the E_a of C−N bond scission by ca. 0.1 eV, and a coadsorbed water molecule nearly spontaneously transfers a hydrogen atom to NH_2 forming NH_3 and OH so hydrogen transfer is included as part of step c + f → h in Table 2. A water molecule in close vicinity of acetamide dissociates spontaneously on (110) and (100), although C−N bond scission that occurs in the presence of a pair of OH and H (step c + g → d + g) on these two facets does not differ much from C−N bond scission in the absence of water (cf. step c → d). C−N bond scission is followed by NH_2 accepting the dissociated H atom to forming NH_3 (step d + g → h), which has an smaller E_a still than the preceding step. The energetic difference between the NH_2 and NH_3 states is the smallest on the (100) facet (Figure 5), making it more likely for the coverage of NH_2 to build up and become detectable on (100).

The acetyl and OH groups stabilize each other strongly, like acetyl and NH_2 (Table S2). The OH group attacks acetyl to form an η^1 acetate coordinated to an H atom (step k → l), i.e., $CH_3COO{-}HO_{latt}$, which amounts to a partially dissociated acetic acid. This state is iso-energetic to the μ acetate coadsorbed with an H atom on an adjacent O_{latt} reported in ref 71. This hydroxylation step has a small E_a (0.17 and 0.23 eV) and exothermic ΔE_{rxn} on (111) and (110), but is endothermic with a sizable E_a (0.78 eV) on (100). The minimum-energy path for this step on all three facets involves the OH group displacing the O_{latt} atom to which acetyl is bonded, that is, in a sense, the OH group pushes an acetate group (i.e., acetyl−O_{latt}) out of the lattice site that it occupies (cf. Figure 4k) and heals the oxygen vacancy that is left behind. Both NH_3 and acetic acid adsorb on the ceria surfaces strongly (cf. Table S1) so that the desorption of the product molecules to the gas phase, particularly acetic acid, (l → m, Table 2) is more rate-limiting than all of the surface elementary steps. This is more so on the (110) and (100) facets than on (111).

We further observe that the reverse of steps l → m, k → l, f → g, and e → f constitutes a reaction channel for acetic acid to reduce the ceria surfaces, which is energetically competitive

https://doi.org/10.1021/acscatal.2c02514
ACS Catal. 2022, 12, 10222−10234

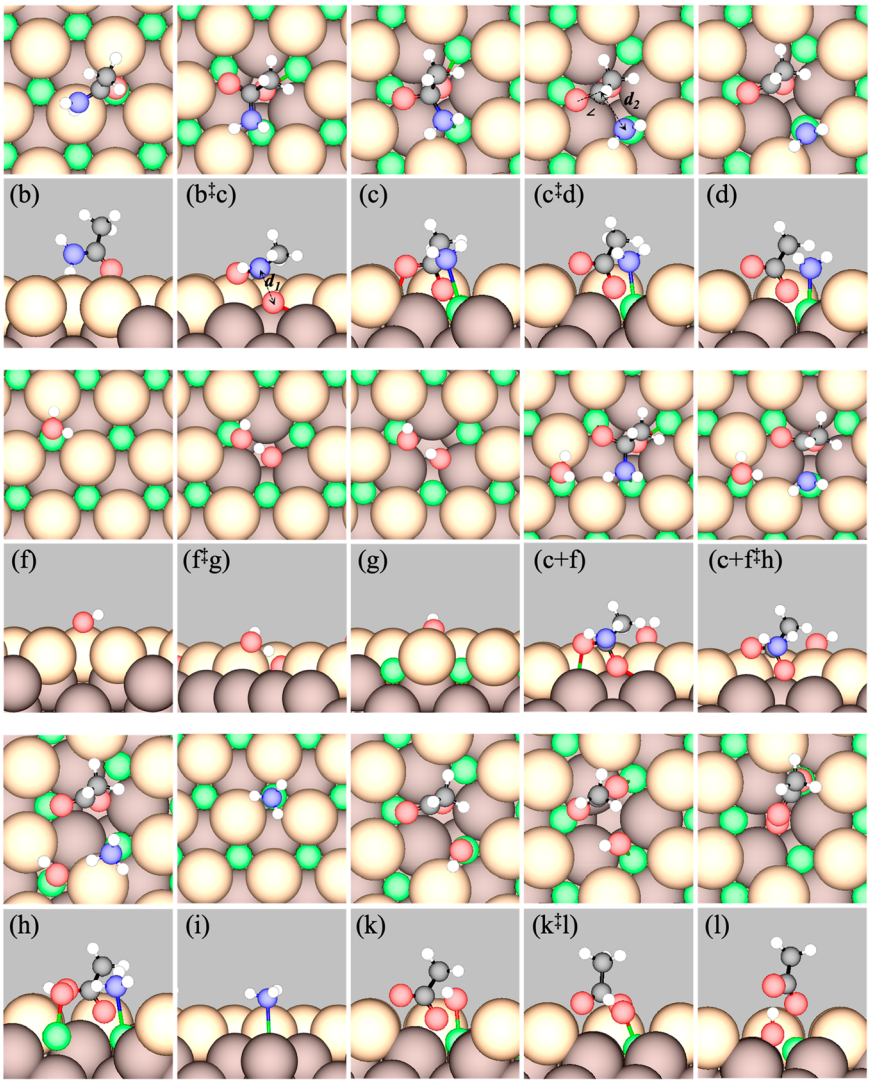

Figure 4. Top (upper panels) and side (lower panels) views of GGA-PW91 optimized stable intermediates and TSs (indicated by ‡) of the elementary steps in deamidation and hydrolysis of acetamide on stoichiometric $CeO_2(111)$. Labels of states correspond to those in Table 2. The states shown are (b) η^1 acetamide, (b‡c) TS of nucleophilic attack by O_{latt}, (c) TI, (c‡d) TS of C−N scission, (d) acetyl + NH_2, (f) H_2O, (f‡g) TS of H_2O dissociation, (g) OH + H, (c + f) TI + H_2O, (c + f‡h) TS of C−N scission with coadsorbed water, (h) acetyl + NH_3 + OH, (i) NH_3, (k) acetyl + OH, (k‡l) TS of OH attack, and (l) acetate + H. [Color code: green, Ce; light brown, surface O_{latt}; dark brown, subsurface O_{latt}; red, O in molecules; black, C; blue, N; and white, H.] O_{latt} bonded to C or H atoms in the molecules are considered part of the molecules. At b‡c, the length of the transitioning C−O_{latt} bond is d_1 = 1.90 Å. At c‡d, the length of the transitioning C−N bond is d_2 = 2.25 Å and the angle ∠OCN is 106.1°.

with acetic acid desorption (Table S3 in the Supporting Information). By removing OH and H as water, a mixture of acetyl and acetate (the other species in step k → l), and not solely acetate, would populate the surface. This surface dehydration channel is not expected to be favorable in aqueous phase based on Le Chatelier's principle, but may become operative when the availability of water is low or nill. This may explain the evolution of water from $CeO_2(111)$ at near-ambient temperature following acetic acid adsorption in the TPD experiments of Calaza et al.[71]

Although the main reaction considered here is the hydrolysis of acetamide, it is worthwhile to remark that an alternate, dehydration pathway exists for acetamide also; see discussion in the Supporting Information. The dehydration of acetamide is energetically not competitive with the deamidation and hydrolysis of acetamide but likewise could become favorable under dry conditions at elevated temperatures.

3.3. Effects of vdW Interaction and Solvation. Our prior work[52,84] suggests that vdW interactions contribute to the stability of organic molecules as small as acetaldehyde when they are adsorbed on ceria. Thus, we have recalculated the minimum-energy reaction energy profiles on the three low-index facets using the optB86b-vdW functional (red dashed traces, Figures 5a−c). Each profile is deepened by vdW interactions on the ΔE axis, particularly for the states in which two molecules are coadsorbed.

Biochemically, deamidation reactions occur in aqueous environments. For ceria functioning as mimics of natural enzymes, an additional possibility of ionized products (NH_4^+ and CH_3COO^-) exists since ammonia and acetic acid are mildly basic and acidic, respectively. We have calculated the free energy of hydration (ΔG_{hyd}) for the reactant and product species, using VASP/VASPsol and QE/Environ. The results are tabulated in Table S4 in the Supporting Information. It can

https://doi.org/10.1021/acscatal.2c02514
ACS Catal. 2022, 12, 10222−10234

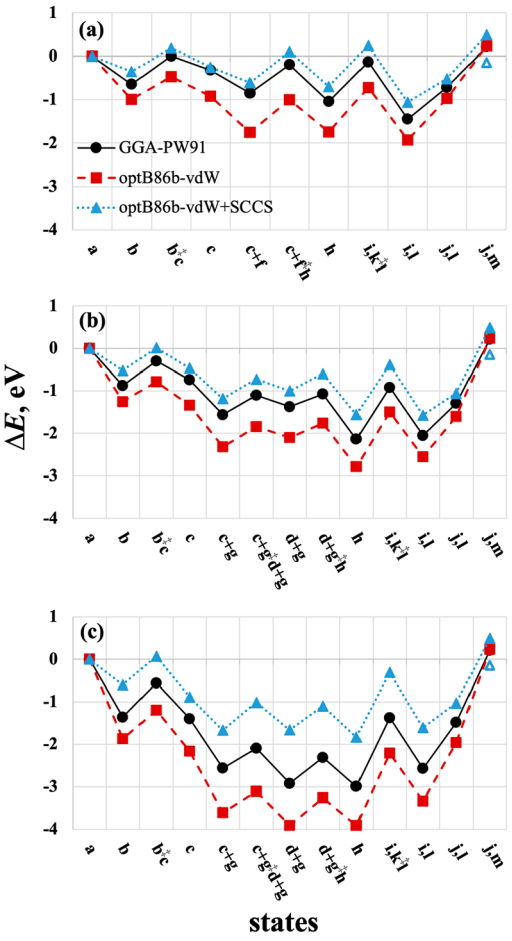

Figure 5. Minimum-energy reaction energy profiles for deamidation and hydrolysis of acetamide on (111), (110), and (100) facets (a–c) respectively, calculated using GGA-PW91 (black circles, VASP), optB86b-vdW (red squares, QE), and optB86b-vdW+SCCS (blue triangles, QE). The reaction states are (a) acetamide, water; (b) η^1 acetamide, (b‡c) TS of nucleophilic attack by O_{latt}; (c) TI; (c + f) TI + H_2O; (c + f‡h) TS of C–N scission + H_2O; (c + g) TI + OH + H; (c + g‡d + g) TS of C–N scission + OH + H; (d + g) acetyl + NH_2 + OH + H; (d + g‡h) TS of NH_2 hydrogenation; (h) acetyl + NH_3 + OH; (i, k‡l) NH_3, TS of OH attack; (i, l) NH_3, acetate + H, (j, l) NH_3 desorbed; and (j, m) acetic acid desorbed. Labels correspond to those in Table 2. Hollow blue triangle in each panel corresponds to aqueous NH_4^+ and CH_3COO^-. The optB86b-vdW profile, when calculated using VASP, differs from QE (red squares) by 0.11 eV or less.

be seen that the two implicit solvation models agree closely with each other, irrespective of the exchange-correlation functional used. For neutral, closed-shell species, our results also agree closely with the values calculated based on the Langevin dipoles solvation model by Warshel and co-workers and with experimental measurements.[106,107] Noticeable deviations are seen for the ionic species, with the theoretical models, particularly VASPsol and Environ, underpredicting solvation for the acetate anion and overpredicting it for the ammonium cation. Since ionic species carry localized charges that are strongly solvated by water, a lack of explicitly description of localized hydrogen bonding by the implicit solvation models is expected to lead to some errors. While the overall deamidation reaction is slightly endothermic and endergonic in the gas phase, the reaction AcD(aq) + H_2O(aq) → NH_4^+(aq) + CH_3COO^-(aq) is computed to be mildly exergonic at −0.18 eV, which is 0.31 eV lower than the ΔG_{rxn} for the gas phase reaction (see Table S5 in the Supporting Information). It suggests that aqueous phase is a thermodynamically necessary condition for the deamidation reaction to occur under ambient conditions. The solvated ionic final product state is indicated by a hollow triangle in Figure 5.

We have then attempted to estimate the effect of hydration on the stability of the surface intermediates in combination with vdW interactions, using the SCCS implicit solvation model implemented in QE/Environ. Solvation by water is predicted to reduce the surface energy of the clean ceria facets by 11, 21, and 25 meV/Å^2 for the (111), (110), and (100) facets, respectively, which is large, compared to, e.g. Pt(111), for which the surface energy is reduced by implicit solvation by water by 2 meV/Å^2.[87] The sizable stabilization is consistent with the fact that ceria surfaces exhibit arrays of localized charge centers, which elicit a strong dielectric response by the solvent, independent of specific chemical or hydrogen bonding interactions between the aqueous phase and the surface.

The adsorption of the reactant and product molecules generally interferes with the interfacial dielectric response of aqueous phase to the ceria surfaces. The solvation of the surfaces is reduced (i.e., positive $\Delta\Delta G_{hyd}$, Table 3) particularly for (100). The exceptions include H_2O on (111), which has no effect on surface solvation, and acetic acid on (111) and (110), which enhances surface solvation. Viewed from a different angle, the adsorption strengths of all the molecules are reduced (i.e., positive $\Delta\Delta E_{ads}$, Table 3), meaning more facile desorption in the aqueous phase than in the gas phase.

Overall, the proposed pathway has a shallower reaction energy profile on (111) than on (110) and (100) when both vdW interaction and solvation effects are taken into account, suggesting the (111) facet to be the most advantageous of the three facets for catalyzing acetamide hydrolysis in aqueous phase based on thermodynamics. TS calculations are not

Table 3. Various Measures of Solvation Effects on Reactant and Product Molecules, Calculated Using optB86b-vdW with QE[a]

		(111)				(110)				(100)			
	ΔG_{hyd} (aq)	ΔE_{ads}	ΔE_{ads}^{SCCS}	$\Delta\Delta G_{hyd}$	$\Delta\Delta E_{ads}$	ΔE_{ads}	ΔE_{ads}^{SCCS}	$\Delta\Delta G_{hyd}$	$\Delta\Delta E_{ads}$	ΔE_{ads}	ΔE_{ads}^{SCCS}	$\Delta\Delta G_{hyd}$	$\Delta\Delta E_{ads}$
η^1-AcD	−0.52	−0.99	−0.35	+0.12	+0.64	−1.25	−0.52	+0.21	+0.73	−1.87	−0.60	+0.75	+1.27
H_2O	−0.36	−0.69	−0.32	+0.01	+0.37	−0.99	−0.46	+0.17	+0.53	−1.19	−0.48	+0.35	+0.71
NH_3	−0.21	−0.96	−0.54	+0.21	+0.43	−0.95	−0.51	+0.23	+0.44	−1.37	−0.58	+0.58	+0.80
acetate + H	−0.41	−1.20	−1.01	−0.22	+0.19	−1.83	−1.55	−0.12	+0.28	−2.19	−1.52	+0.27	+0.67

[a]Acetic acid is present as an acetate + H pair on the three facets. Differences in optB86b-vdW ΔE_{ads} calculated using VASP (reported in Table S1) vs QE are 0.11 eV or less in all cases. $\Delta G_{hyd\ (aq)}$ = free energy of hydration for molecules in aqueous phase; $\Delta\Delta G_{hyd}$ = change in free energy of hydration for surface with adsorbate vs bare surface; $\Delta\Delta E_{ads}$ = decrease in adsorption strength due to hydration, i.e., amount by which desorption becomes more facile; $\Delta\Delta E_{ads} = \Delta\Delta G_{hyd} - \Delta G_{hyd\ (aq)} = \Delta E_{ads}^{SCCS} - \Delta E_{ads}$

https://doi.org/10.1021/acscatal.2c02514
ACS Catal. 2022, 12, 10222−10234

repeated with vdW interaction and solvation effects included due to convergence difficulties. Instead, we make the assumption that the vdW and solvation effects on a TS are the average of these effects on the IS and FS of an elementary step. This approach would yield errors of 0−0.15 eV for the stability of TS based on the results of our previous study on aldol condensation of acetaldehyde on CeO_2(111).[84] Under this assumption, conversion from the η^1 state to the TI is seen to be slightly outcompeted by acetamide desorption on all three facets, of which the (110) facet is the most efficient at directing a given molecular flux toward acetamide deamidation versus acetamide desorption, followed by (100), and then (111). On the other hand, the adsorption energy of acetic acid (ΔE_{ads}^{SCCS}, Table 3) remains at −1 eV on (111) and lower on (110) and (100) (ΔE_{ads}^{SCCS}, Table 3), suggesting that product desorption continues to be limiting, particularly on the two more open facets, even when assisted by an aqueous phase. A strategy that modifies the C−N bond scission activity and acetate adsorption strength differently will be needed to further optimize an oxide-based catalyst including ceria for the reaction. Once desorbed, acetic acid and NH_3 can undergo acid−base neutralization by ionizing, which provides the thermodynamic driving force for the overall reaction.

3.4. Decomposition of Amides, Amidines, and Generalized Esters on Ceria. The activation and dissociation of the C−N bond over Ce−O_{latt}−Ce sites are not limited to acetamide. We demonstrate this for several other amine compounds, including benzamide, *N*-methylacetamide, acetamidine, and adenine. The reaction energy profiles up to C−N bond scission for these amine compounds on CeO_2(111) are plotted in Figure 6 for comparison with acetamide. The

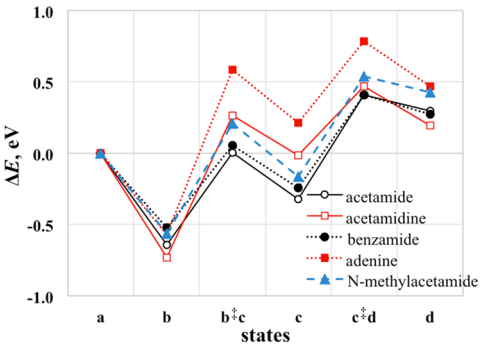

Figure 6. GGA-PW91 reaction energy profiles up to C−N bond scission in various amine compounds on CeO_2(111). The surface reaction states are (a) gas-phase molecule, (b) η^1 state, (b‡c) TS of nucleophilic attack by O_{latt}, (c) TI, (c‡d) TS of C−N scission, and (d) C−N scission products.

immediate fragments that result are benzoyl + NH_2 (for benzamide), acetyl + CH_3NH (for *N*-methylacetamide), CH_3CNH + NH_2 (for acetamidine), and purine + NH_2 (for adenine). These fragments also mutually stabilize on the surface (Table S2). Secondary or tertiary amides (e.g., *N*-methylacetamide) produce amines instead of ammonia.

Benzamide and *N*-methylacetamide can be viewed as derivatives of acetamide. Benzamide has the methyl group in acetamide replaced with a phenyl group, whereas *N*-methylacetamide is obtained by replacing one of the amine hydrogen atoms with a methyl group, making it perhaps the simplest model for peptide bonds in proteins.[108] Acetamidine is a simple amidine, an imine analog of an amide with the C═O group replaced with a C═NH group. These molecules are likewise open to nucleophilic attack by O_{latt} of ceria at the carbonyl C to form TI and then undergo C−N bond scission, with E_a similar to that for acetamide (Figure 6) except for one.

Previously, we studied the adsorption of a primary nucleobase, adenine, on CeO_2(111) as a model system for organic/inorganic interfaces.[52] Adenine can be viewed as a cyclic amidine in which the C═NH group is a part of an aromatic ring. In nature, adenine deaminase catalyzes the conversion of adenine to NH_3 and hypoxanthine. The enzyme contains a binuclear metal center of two Fe^{2+}, which stabilizes a hydroxide group that attacks the C6 position of adenine, the carbon atom to which $-NH_2$ is attached, and replaces the amine group.[92] On CeO_2(111), because of the aromaticity of the purine group, nucleophilic attack by O_{latt} at the C6 position forming TI has a notably higher E_a value (1.16 eV) than in the other compounds, but is followed by a more modest E_a value for C−N bond scission than in acetamide (0.48 eV).

The C−N bond scission steps for acetamide, benzamide, *N*-methylacetamide, acetamidine, and adenine are analyzed in terms of a linear energy relationship between the TS and the FS.[109,110] To this dataset, we also add the results for several other examples of generalized esters (GEs), which all contain the X(═Y)−Z moiety, where Y and Z are more electronegative atoms than X, resulting in a polarized X−Z generalized ester bond (Figure 7). The additional GEs include

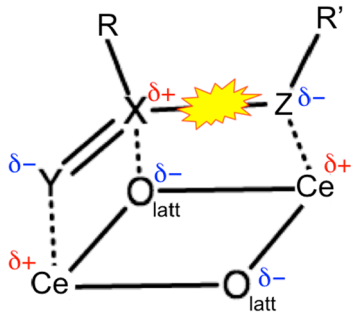

Figure 7. Schematic illustrating how a generalized ester (RX(═Y)−ZR′) interacts with an ensemble of Ce−O_{latt}−Ce surface sites. The generalized ester bond is highlighted.

methyl formate and methyl acetate (X═C, Y═Z═O), and phenyl phosphate, *para*-nitrophenyl phosphate, *para*-chlorophenyl phosphate, and chloromethyl phosphate (X═P, Y═Z═O) that are taken from our previous work on phosphate monoesters on CeO_2(111).[94,95] The results for acetamide, acetamidine, and methyl acetate on the (110) and (100) facets are also included, for which the dissociated fragments of RX═Y and ZR′ are notably more stable than on (111). When the stability of the TS of the X−Z bond scission is plotted against that of the FS for this diverse group of GEs, a linear Brønsted−Evans−Polanyi relationship is obtained (Figure 8a). The TS for the carboxylates and phosphates on (111), and for all the compounds considered on (110) and (100), lie below 0 eV versus the gas phase, which suggests ceria to be a potentially effective catalyst for de-esterification of such compounds. This is consistent with previous theoretical studies that report low E_a for the scission of ester bonds in other examples of GEs including dimethylcarbonate[93] and dimethyl methylphosphonate.[111] Using this linear relationship, one may quickly

https://doi.org/10.1021/acscatal.2c02514
ACS Catal. 2022, 12, 10222−10234

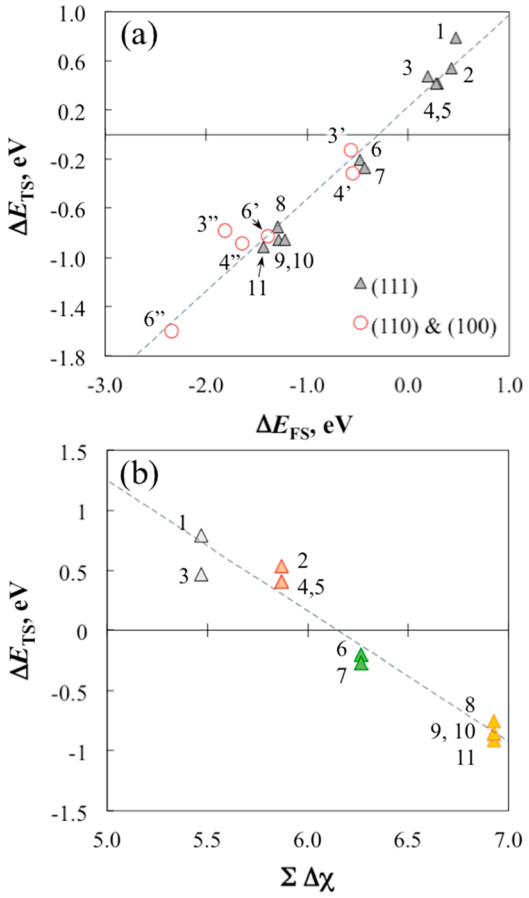

Figure 8. (a) GGA-PW91 stability of the TS versus the FS (coadsorbed dissociated fragments) of the scission of X−Z generalized ester bond, and (b) stability of the TS versus the electronegativity-based descriptor, $\sum\Delta\chi$, for several GEs on $CeO_2(111)$. The compounds included are adenine (1), *N*-methylacetamide (2), acetamidine (3), acetamide (4), benzamide (5), methyl acetate (6), methyl formate (7), chloromethyl phosphate (8), *para*-chlorophenyl phosphate (9), and phenyl phosphate (10), and *para*-nitrophenyl phosphate (11). Unmarked numbers indicate results on (111), single prime symbol (′) indicates results on (110), and double prime symbol (″) indicates results on (100). The TS and FS of the phosphates are those that do not involve spontaneous dissociation of an acidic proton. Data values are listed in Table S6 in the Supporting Information, and snapshots of the TS are shown in Figure S4 in the Supporting Information. The lines are results of linear regression: in panel (a), $\Delta E_{TS} = 0.750\ \Delta E_{FS} + 0.226$, $R^2 = 0.958$; in panel (b), $\Delta E_{TS} = -1.086\ \sum\Delta\chi + 6.677$, $R^2 = 0.956$ with $a = 1.83$.

estimate the stability of the TS of the scission of the generalized ester bond in GEs.

The data in Figure 8a cluster in separate groups for phosphates, carboxylates, and amides/amidines on a given facet. This clustering hints at underlying, systematic factors that influence the stability of the surface complexes that these organic compounds form on ceria. For acetamide and the related compounds, the carbonyl C−O_{latt} bond obviously plays an important role in the stability of the TS of C−N bond scission on the ceria surfaces. At the same time, the carbonyl O and the amine N atoms are coordinated to adjacent Ce sites, but how strong the O(N)−Ce interaction is versus the C−O_{latt} bond is unclear. We surmise that the nature of the X, Y, and Z atoms in a GE that correspond to the ensemble of Ce−O_{latt}−Ce surface sites determines the stability of the TS for a given GE on $CeO_2(111)$. Inspired by Capdevila-Cortada et al.,[96] we propose a descriptor to measure this interaction, which is based on the electronegativity (χ_i) of the atoms involved:

$$\sum \Delta\chi = a|\chi_O - \chi_X| + |\chi_{Ce} - \chi_Y| + |\chi_{Ce} - \chi_Z|$$

We use the Pauling electronegativity for the elements involved, i.e., $\chi_{Ce} = 1.12$, $\chi_C = 2.55$, $\chi_N = 3.04$, $\chi_O = 3.44$, and $\chi_P = 2.19$. a is an adjustable parameter to represent different weighting of the X−O_{latt} bonding relative to the interaction between the Y and Z atoms and Ce. The stability of the TS for the scission of the X−Z generalized ester bond on $CeO_2(111)$ included in Figure 8a is replotted against $\sum\Delta\chi$ in Figure 8b. While this simple descriptor does not account for the chemical environment beyond the X(═Y)−Z moiety or the catalytic site structure, Figure 8b suggests that it captures the trend in the stability of the TS, which supports our hypothesis. The optimized value of a is 1.83, indicating that the X−O_{latt} bond is notably stronger than the interaction between the Y or Z atom and Ce^{4+}. The different coordination environment and geometry of the Ce−O_{latt}−Ce ensemble would account for the different reactivity of the facets toward the decomposition of GEs.

Of the two fragments that are produced upon scission of the generalized ester bond, the ZR′ fragment is hydrogenated into an alcohol or amine/NH_3, while the RX(═Y) fragment is hydroxylated into RX(═Y)OH that is tautomeric with RX(═O)YH. Conceivably, if RX(═Y)OH is not tied up in an aromatic moiety (e.g., adenine), it could undergo hydrolysis again until all X−Y bonds (when Y ≠ O) are replaced by X−O bonds to produce the corresponding acid (RXOOH); e.g., acetamidine fully hydrolyzed to acetic acid. Based on the examples used in Figure 8, we further compare the ΔE_{ads} values of several carboxylic acids, including formic, acetic, and benzoic acids, on $CeO_2(111)$. The difference in ΔE_{ads} values turns out to be noticeable in the gas phase but less pronounced at the water/solid interface (see Figure S5 in the Supporting Information).

4. CONCLUSIONS

Ceria has been regarded as enzyme-mimicking because it exhibits catalytic activity under ambient conditions for the decomposition via hydrolysis of a range of organic compounds including carboxylates, phosphates, and amides, which is reminiscent of the action of natural metallohydrolases, including phosphatase and peptidase, that use metal ions to catalyze the hydrolysis of many biological compounds of the same types. We have performed periodic DFT calculations to investigate the mechanism and energetics of deamidation via hydrolysis on the three low-index CeO_2 facets, (111), (110), and (100), using acetamide as the main model compound.

The reaction shares similar features on the three facets, of which (111) is the least reactive and binds reaction intermediates least strongly while (100) is the most reactive. Acetamide adsorbs molecularly with its carbonyl O coordinated to a Ce cation and one of its amine H coordinated to an adjacent lattice O anion. The amide C−N bond scission is preceded by the formation of a tetrahedral intermediate (TI) state, formed via nucleophilic attack by lattice O on the carbonyl C, which has an activation barrier of $E_a = 0.65$, 0.57, and 0.80 eV on the (111), (110), and (100) facets, respectively. In the presence of a water molecule, C−N

https://doi.org/10.1021/acscatal.2c02514
ACS Catal. 2022, 12, 10222−10234

scission in the TI occurs with a more modest barrier (E_a = 0.65, 0.46, and 0.47 eV on (111), (110), and (100)), producing acetyl and NH_2 fragments. NH_2 readily extracts a hydrogen atom from water to form NH_3. The remaining OH group attacks acetyl to form an acetate + H pair, which is facile on (111) (E_a = 0.17 eV) but has a more substantial barrier on (100) (E_a = 0.78 eV). The overall reaction is desorption-limited in the gas phase, particularly for acetic acid on the two more open facets. The calculated desorption energies for NH_3 and acetic acid are 0.74 and 0.93 eV on (111), 0.76 and 1.51 eV on (110), and 1.09 and 1.70 eV on (100). These values are larger than the calculated E_a values for all the surface reaction steps in the minimum-energy reaction mechanism on the respective facets.

Since biologically and environmentally relevant deamidation reactions occur in the aqueous phase, we have further used the SCCS implicit solvent model in combination with van der Waals corrections to estimate the reaction energetics at the aqueous interface. While vdW interactions stabilize the surface intermediates, the implicit solvent has the opposite effect and makes the reaction energy profiles less corrugated than in the gas phase. Desorption of all reactant and product species is predicted to be enhanced by the aqueous phase, although the desorption of acetic acid is expected to remain kinetically hindered at ambient temperature.

A survey of the literature and our own studies suggest that the Ce−O_{latt}−Ce site ensembles present on ceria surfaces are well-suited to activating organic moieties of the X(═Y)−Z type, in which Y and Z are more electronegative atoms than X, resulting in a polarized X−Z bond. We term such compounds generalized esters (GEs), which includes carboxylates, phosphates, and amides among many others. A simple descriptor ($\sum\Delta\chi$) is proposed that takes into account the electronegativity of both the atoms constituting the bond (X, Z) and those of the catalytic site (Ce, O). It captures a linear trend in the stability of the TS of X−Z bond scission on CeO_2(111), revealing a connection between the composition of the oxide surface and the catalytic activity for the decomposition of GEs.

Our work identifies certain factors that will need to be addressed in future catalyst design based on ceria and other metal compounds for catalytic decomposition of a wide range of organic and biologically active compounds, such as those controlling the catalytic activity for cleaving generalized ester bonds and the rate-limiting desorption of carboxylate products. The findings are also relevant to ceria- and oxide-catalyzed generalized esterification and trans-esterification reactions, which involve the formation instead of scission of generalized ester bonds.[46,93,112]

■ ASSOCIATED CONTENT

Supporting Information

The Supporting Information is available free of charge at https://pubs.acs.org/doi/10.1021/acscatal.2c02514.

Comparison of adsorption energies of reaction reactants and products on CeO_2(111), (110), and (100) with literature values; interaction energies of reaction intermediates on CeO_2(111), (110), and (100); comparison of reaction energies for the desorption of water compared to desorption of acetic acid on CeO_2(111), (110), and (100); comparison of free energies of hydration of reactant and product species with literature values; overall total and free energies for acetamide hydrolysis; tabulated data used in Figure 8; simulated vibrational spectra of acetamide adsorbed on CeO_2(111), (110), and (100); snapshots of stable intermediates and transition states of the elementary steps in deamidation and hydrolysis of acetamide on stoichiometric CeO_2(110) and (100) facets; snapshots of transition states of X−Z bond scission in GEs on CeO_2(111), (110), and (100); adsorption energies of several carboxylic acids on CeO_2(111); results and discussion on acetamide dehydration on CeO_2(111), (110), and (100) (PDF)

■ AUTHOR INFORMATION

Corresponding Author

Ye Xu − *Cain Department of Chemical Engineering, Louisiana State University, Baton Rouge, Louisiana 70803, United States;* orcid.org/0000-0002-6406-7832; Email: yexu@lsu.edu

Author

Suman Bhasker-Ranganath − *Cain Department of Chemical Engineering, Louisiana State University, Baton Rouge, Louisiana 70803, United States;* Present Address: SUNCAT Center for Interface Science and Catalysis, SLAC National Accelerator Laboratory, Menlo Park, California 94025, United States

Complete contact information is available at: https://pubs.acs.org/10.1021/acscatal.2c02514

Notes

The authors declare no competing financial interest.

■ ACKNOWLEDGMENTS

This work was supported by the U.S. National Science Foundation, under Grant No. CHE-1664984, and used high performance computational resources provided by Louisiana State University, by the Center for Nanophase Materials Sciences, which is a DOE Office of Science User Facility, and by the National Energy Research Scientific Computing Center, which is supported by the Office of Science of US-DOE (under Contract No. DE-AC02-05CH11231).

■ REFERENCES

(1) Greenberg, A.; Brenemen, C.; Liebman, J. *The Amide Linkage: Structural Significance in Chemistry, Biochemistry, and Materials Science*; John Wiley & Sons, 2000.

(2) Kemnitz, C. R.; Loewen, M. J. "Amide Resonance" correlates with a breadth of C−N rotation barriers. *J. Am. Chem. Soc.* **2007**, *129*, 2521−2528.

(3) Bender, M. L. Mechanisms of catalysis of nucleophilic reactions of carboxylic acid derivatives. *Chem. Rev.* **1960**, *60*, 53−113.

(4) O'Connor, C. Acidic and basic amide hydrolysis. *Q. Rev. Chem. Soc.* **1970**, *24*, 553−564.

(5) Hine, J.; King, R. S. M.; Midden, W. R.; Sinha, A. Hydrolysis of formamide at 80 °C and pH 1−9. *J. Org. Chem.* **1981**, *46*, 3186−3189.

(6) Robinson, B. A.; Tester, J. W. Kinetics of alkaline hydrolysis of organic esters and amides in neutrally-buffered solution. *Int. J. Chem. Kinet.* **1990**, *22*, 431−448.

(7) Bakowies, D.; Kollman, P. A. Theoretical study of base-catalyzed amide hydrolysis: Gas- and aqueous-phase hydrolysis of formamide. *J. Am. Chem. Soc.* **1999**, *121*, 5712−5726.

(8) Bender, M. L.; Pollack, R. M. Alkaline hydrolysis of p-nitroacetanilide and p-formylacetanilide. *J. Am. Chem. Soc.* **1970**, *92*, 7190−7194.
(9) Radzicka, A.; Wolfenden, R. Rates of uncatalyzed peptide bond hydrolysis in neutral solution and the transition state affinities of proteases. *J. Am. Chem. Soc.* **1996**, *118*, 6105−6109.
(10) Smith, R. M.; Hansen, D. E. The pH-rate profile for the hydrolysis of a peptide bond. *J. Am. Chem. Soc.* **1998**, *120*, 8910−8913.
(11) Sayre, L. M. Metal ion catalysis of amide hydrolysis. *J. Am. Chem. Soc.* **1986**, *108*, 1632−1635.
(12) Christianson, D. W.; Lipscomb, W. N. Carboxypeptidase A. *Acc. Chem. Res.* **1989**, *22*, 62−69.
(13) Kilshtain, A. V.; Warshel, A. On the origin of the catalytic power of carboxypeptidase A and other metalloenzymes. *Proteins Struct. Funct. Bioinform.* **2009**, *77*, 536−550.
(14) Mahesh, S.; Tang, K.-C.; Raj, M. Amide bond activation of biological molecules. *Molecules* **2018**, *23*, 2615.
(15) Yashiro, M.; Sonobe, Y.; Yamamura, A.; Takarada, T.; Komiyama, M.; Fujii, Y. Metal-ion-assisted hydrolysis of dipeptides involving a serine residue in a neutral aqueous solution. *Org. Biomol. Chem.* **2003**, *1*, 629−632.
(16) Mihaylov, T. T.; Parac-Vogt, T. N.; Pierloot, K. A mechanistic study of the spontaneous hydrolysis of glycylserine as the simplest model for protein self-cleavage. *Chem. − Eur. J.* **2014**, *20*, 456−466.
(17) Grant, K.; Kassai, M. Major advances in the hydrolysis of peptides and proteins by metal ions and complexes. *Curr. Org. Chem.* **2006**, *10*, 1035−1049.
(18) Wezynfeld, N. E.; Frączyk, T.; Bal, W. Metal assisted peptide bond hydrolysis: Chemistry, biotechnology and toxicological implications. *Coord. Chem. Rev.* **2016**, *327*−*328*, 166−187.
(19) Hegg, E. L.; Burstyn, J. N. Hydrolysis of unactivated peptide bonds by a macrocyclic copper(II) complex: Cu([9]aneN$_3$)Cl$_2$ hydrolyzes both dipeptides and proteins. *J. Am. Chem. Soc.* **1995**, *117*, 7015−7016.
(20) Fujii, Y.; Kiss, T.; Gajda, T.; Tan, X.; Sato, T.; Nakano, Y.; Hayashi, Y.; Yashiro, M. Copper(II)-cis,cis-1,3,5-triaminocyclohexane complex-promoted hydrolysis of dipeptides: Kinetic, speciation and structural studies. *J. Biol. Inorg. Chem.* **2002**, *7*, 843−851.
(21) Parac, T. N.; Kostić, N. M. New selectivity and turnover in peptide hydrolysis by metal complexes. A palladium(II) aqua complex catalyzes cleavage of peptides next to the histidine residue. *J. Am. Chem. Soc.* **1996**, *118*, 51−58.
(22) Zhu, L.; Kostic, N. M. Toward artificial metallopeptidases: Mechanisms by which platinum(II) and palladium(II) complexes promote selective, fast hydrolysis of unactivated amide bonds in peptides. *Inorg. Chem.* **1992**, *31*, 3994−4001.
(23) Chei, W. S.; Ju, H.; Suh, J. New chelating ligands for Co(III)-based peptide-cleaving catalysts selective for pathogenic proteins of amyloidoses. *J. Biol. Inorg. Chem.* **2011**, *16*, 511−519.
(24) Kita, Y.; Nishii, Y.; Higuchi, T.; Mashima, K. Zinc-catalyzed amide cleavage and esterification of β-hydroxyethylamides. *Angew. Chem., Int. Ed.* **2012**, *51*, 5723−5726.
(25) Yashiro, M.; Sonobe, Y.; Yamamura, A.; Takarada, T.; Komiyama, M.; Fujii, Y. Metal-ion-assisted hydrolysis of dipeptides involving a serine residue in a neutral aqueous solution. *Org. Biomol. Chem.* **2003**, *1*, 629−632.
(26) Bamann, E.; Rother, A.; Trapmann, H. Metallkatalytische Losung der Peptidbindung. *Naturwissenschaften* **1956**, *43*, 326−326.
(27) Bamann, E.; Trapmann, H.; Rother, A. About the hydrolysis of dipeptides in the presence of lanthanum, cerium (III), and cerium (IV) ions. *Chem. Ber.* **1958**, *91*, 1744−1751.
(28) Yashiro, M.; Takarada, T.; Miyama, S.; Komiyama, M. Cerium(IV)−cyclodextrin complex for peptide hydrolysis in neutral homogeneous solutions. *J. Chem. Soc., Chem. Commun.* **1994**, *2*, 1757−1758.
(29) Takarada, T.; Yashiro, M.; Komiyama, M. Catalytic hydrolysis of peptides by cerium(IV). *Chem. − Eur. J.* **2000**, *6*, 3906−3913.
(30) Stroobants, K.; Moelants, E.; Ly, H. G. T.; Proost, P.; Bartik, K.; Parac-Vogt, T. N. Polyoxometalates as a novel class of artificial proteases: Selective hydrolysis of lysozyme under physiological pH and temperature promoted by a cerium(IV) Keggin-type polyoxometalate. *Chem. — Eur. J.* **2013**, *19*, 2848−2858.
(31) Sap, A.; Van Tichelen, L.; Mortier, A.; Proost, P.; Parac-Vogt, T. N. Tuning the selectivity and reactivity of metal-substituted polyoxometalates as artificial proteases by varying the nature of the embedded Lewis acid metal ion. *Eur. J. Inorg. Chem.* **2016**, *2016*, 5098−5105.
(32) Quanten, T.; De Mayaer, T.; Shestakova, P.; Parac-Vogt, T. N. Selectivity and reactivity of ZrIV and CeIV substituted Keggin type polyoxometalates toward cytochrome c in surfactant solutions. *Front. Chem.* **2018**, *6*, 1−13.
(33) Moons, J.; Van Rompuy, L. S.; Rodriguez, A.; Abdelhameed, S. A. M.; Simons, W.; Parac-Vogt, T. N. Hydrolysis of transferrin promoted by a cerium(IV)-Keggin polyoxometalate. *Polyhedron* **2019**, *170*, 570−575.
(34) Siddiki, S. M. A. H.; Touchy, A. S.; Tamura, M.; Shimizu, K. Versatile and sustainable alcoholysis of amides by a reusable CeO_2 catalyst. *RSC Adv.* **2014**, *4*, 35803−35807.
(35) Kamachi, T.; Siddiki, S. M. A. H.; Morita, Y.; Rashed, M. N.; Kon, K.; Toyao, T.; Shimizu, K.; Yoshizawa, K. Combined theoretical and experimental study on alcoholysis of amides on CeO_2 surface: A catalytic interplay between Lewis acid and base sites. *Catal. Today* **2018**, *303*, 256−262.
(36) Rashed, M. N.; Siddiki, S. M. A. H.; Touchy, A. S.; Jamil, M. A. R.; Poly, S. S.; Toyao, T.; Maeno, Z.; Shimizu, K. Direct phenolysis reactions of unactivated amides into phenolic esters promoted by a heterogeneous CeO_2 catalyst. *Chem. − Eur. J.* **2019**, *25*, 10594−10605.
(37) Toyao, T.; Nurnobi Rashed, M.; Morita, Y.; Kamachi, T.; Hakim Siddiki, S. M. A.; Ali, M. A.; Touchy, A. S.; Kon, K.; Maeno, Z.; Yoshizawa, K.; Shimizu, K. Esterification of tertiary amides by alcohols through C−N bond cleavage over CeO_2. *ChemCatChem.* **2019**, *11*, 449−456.
(38) Siddiki, S. M. A. H. A. H.; Rashed, M. N.; Touchy, A. S.; Jamil, M. A. R. R.; Jing, Y.; Toyao, T.; Maeno, Z.; Shimizu, K. I. Hydrolysis of amides to carboxylic acids catalyzed by Nb_2O_5. *Catal. Sci. Technol.* **2021**, *11*, 1949−1960.
(39) Zhang, D.; Du, X.; Shi, L.; Gao, R. Shape-controlled synthesis and catalytic application of ceria nanomaterials. *Dalton Trans.* **2012**, *41*, 14455−14475.
(40) Qiao, Z. A.; Wu, Z.; Dai, S. Shape-controlled ceria-based nanostructures for catalysis applications. *ChemSusChem* **2013**, *6*, 1821−1833.
(41) Huang, W.; Gao, Y. Morphology-dependent surface chemistry and catalysis of CeO_2 nanocrystals. *Catal. Sci. Technol.* **2014**, *4*, 3772−3784.
(42) Trovarelli, A.; Llorca, J. Ceria catalysts at nanoscale: How Do crystal shapes shape catalysis? *ACS Catal.* **2017**, *7*, 4716−4735.
(43) Mullins, D. R.; Albrecht, P. M.; Calaza, F. Variations in reactivity on different crystallographic orientations of cerium oxide. *Top. Catal.* **2013**, *56*, 1345−1362.
(44) Wu, Z.; Li, M.; Overbury, S. H. On the structure dependence of CO oxidation over CeO_2 nanocrystals with well-defined surface planes. *J. Catal.* **2012**, *285*, 61−73.
(45) Li, M.; Wu, Z.; Overbury, S. H. Surface structure dependence of selective oxidation of ethanol on faceted CeO_2 nanocrystals. *J. Catal.* **2013**, *306*, 164−176.
(46) Laursen, S.; Combita, D.; Hungría, A. B.; Boronat, M.; Corma, A. First-principles design of highly active and selective catalysts for phosgene-free synthesis of aromatic polyurethanes. *Angew. Chem., Int. Ed.* **2012**, *51*, 4190−4193.
(47) Wang, S.; Zhao, L.; Wang, W.; Zhao, Y.; Zhang, G.; Ma, X.; Gong, J. Morphology control of ceria nanocrystals for catalytic conversion of CO_2 with methanol. *Nanoscale* **2013**, *5*, 5582.
(48) Manto, M. J.; Xie, P.; Wang, C. Catalytic dephosphorylation using ceria nanocrystals. *ACS Catal.* **2017**, *7*, 1931−1938.

https://doi.org/10.1021/acscatal.2c02514
ACS Catal. 2022, 12, 10222−10234

(49) Nolan, M.; Parker, S. C.; Watson, G. W. The electronic structure of oxygen vacancy defects at the low index surfaces of ceria. *Surf. Sci.* **2005**, *595*, 223−232.
(50) Paier, J.; Penschke, C.; Sauer, J. Oxygen defects and surface chemistry of ceria: Quantum chemical studies compared to experiment. *Chem. Rev.* **2013**, *113*, 3949−3985.
(51) Gaded, V.; Anand, R. Nucleobase deaminases: A potential enzyme system for new therapies. *RSC Adv.* **2018**, *8*, 23567−23577.
(52) Bercha, S.; Bhasker-Ranganath, S.; Zheng, X.; Beranová, K.; Vorokhta, M.; Acres, R. G.; Skála, T.; Matolín, V.; Prince, K. C.; Xu, Y.; Tsud, N. Adsorption structure of adenine on cerium oxide. *Appl. Surf. Sci.* **2020**, *530*, 147257.
(53) Candanosa, R. M. How nanoparticles could help us get closer to a treatment for COVID-19. *News@Northeastern*, 2020. Available via the Internet at: https://research.northeastern.edu/heres-how-nanoparticles-could-help-us-get-closer-to-a-treatment-for-covid-19/.
(54) Perdew, J.; Chevary, J.; Vosko, S.; Jackson, K.; Pederson, M.; Singh, D.; Fiolhais, C. Atoms, molecules, solids, and surfaces: Applications of the generalized gradient approximation for exchange and correlation. *Phys. Rev. B* **1992**, *46*, 6671−6687.
(55) Dion, M.; Rydberg, H.; Schröder, E.; Langreth, D. C.; Lundqvist, B. I. Van der Waals density functional for general geometries. *Phys. Rev. Lett.* **2004**, *92*, 246401.
(56) Román-Pérez, G.; Soler, J. M. Efficient implementation of a van der Waals density functional: Application to double-wall carbon nanotubes. *Phys. Rev. Lett.* **2009**, *103*, 096102.
(57) Klimeš, J.; Bowler, D. R.; Michaelides, A. Chemical accuracy for the van der Waals density functional. *J. Phys.: Condens. Matter* **2010**, *22*, 022201.
(58) Klimes, J.; Bowler, D. R.; Michaelides, A. Van der Waals density functionals applied to solids. *Phys. Rev. B - Condens. Matter Mater. Phys.* **2011**, *83*, 195131.
(59) Kresse, G.; Hafner, J. Ab initio molecular dynamics for liquid metals. *Phys. Rev. B* **1993**, *47*, 558−561.
(60) Kresse, G.; Hafner, J. Ab initio molecular-dynamics simulation of the liquid-metal−amorphous-semiconductor transition in germanium. *Phys. Rev. B* **1994**, *49*, 14251−14269.
(61) Kresse, G.; Furthmüller, J. Efficient iterative schemes for ab initio total-energy calculations using a plane-wave basis set. *Phys. Rev. B* **1996**, *54*, 11169−11186.
(62) Kresse, G.; Furthmüller, J. Efficiency of ab-initio total energy calculations for metals and semiconductors using a plane-wave basis set. *Comput. Mater. Sci.* **1996**, *6*, 15−50.
(63) Giannozzi, P.; Baroni, S.; Bonini, N.; Calandra, M.; Car, R.; Cavazzoni, C.; Ceresoli, D.; Chiarotti, G. L.; Cococcioni, M.; Dabo, I.; Dal Corso, A.; de Gironcoli, S.; Fabris, S.; Fratesi, G.; Gebauer, R.; Gerstmann, U.; Gougoussis, C.; Kokalj, A.; Lazzeri, M.; Martin-Samos, L.; Marzari, N.; Mauri, F.; Mazzarello, R.; Paolini, S.; Pasquarello, A.; Paulatto, L.; Sbraccia, C.; Scandolo, S.; Sclauzero, G.; Seitsonen, A. P.; Smogunov, A.; Umari, P.; Wentzcovitch, R. M. QUANTUM ESPRESSO: A modular and open-source software project for quantum simulations of materials. *J. Phys.: Condens. Matter* **2009**, *21*, 395502.
(64) Giannozzi, P.; Andreussi, O.; Brumme, T.; Bunau, O.; Buongiorno Nardelli, M.; Calandra, M.; Car, R.; Cavazzoni, C.; Ceresoli, D.; Cococcioni, M.; Colonna, N.; Carnimeo, I.; Dal Corso, A.; de Gironcoli, S.; Delugas, P.; DiStasio, R. A.; Ferretti, A.; Floris, A.; Fratesi, G.; Fugallo, G.; Gebauer, R.; Gerstmann, U.; Giustino, F.; Gorni, T.; Jia, J.; Kawamura, M.; Ko, H.-Y.; Kokalj, A.; Küçükbenli, E.; Lazzeri, M.; Marsili, M.; Marzari, N.; Mauri, F.; Nguyen, N. L.; Nguyen, H.-V.; Otero-de-la-Roza, A.; Paulatto, L.; Poncé, S.; Rocca, D.; Sabatini, R.; Santra, B.; Schlipf, M.; Seitsonen, A. P.; Smogunov, A.; Timrov, I.; Thonhauser, T.; Umari, P.; Vast, N.; Wu, X.; Baroni, S. Advanced capabilities for materials modelling with Quantum ESPRESSO. *J. Phys.: Condens. Matter* **2017**, *29*, 465901.
(65) Blöchl, P. E. Projector augmented-wave method. *Phys. Rev. B* **1994**, *50*, 17953−17979.
(66) Kresse, G.; Joubert, D. From ultrasoft pseudopotentials to the projector augmented-wave method. *Phys. Rev. B* **1999**, *59*, 1758−1775.
(67) Prandini, G.; Marrazzo, A.; Castelli, I. E.; Mounet, N.; Passaro, E.; Marzari, N. A standard solid state pseudopotentials (SSSP) library optimized for precision and efficiency (Version v7). *Mater. Cloud Arch.* **2021**, 2021.76, DOI: 10.24435/materialscloud:rz-77.
(68) Monkhorst, H. J.; Pack, J. D. Special points for Brillouin-zone integrations. *Phys. Rev. B* **1976**, *13*, 5188−5192.
(69) Li, H.-Y.; Wang, H.-F.; Guo, Y.-L.; Lu, G.-Z.; Hu, P. Exchange between sub-surface and surface oxygen vacancies on CeO_2(111): A new surface diffusion mechanism. *Chem. Commun.* **2011**, *47*, 6105.
(70) Hansen, H. A.; Wolverton, C. Kinetics and thermodynamics of H_2O dissociation on reduced CeO_2(111). *J. Phys. Chem. C* **2014**, *118*, 27402−27414.
(71) Calaza, F. C.; Chen, T.-L.; Mullins, D. R.; Xu, Y.; Overbury, S. H. Reactivity and reaction intermediates for acetic acid adsorbed on CeO_2(111). *Catal. Today* **2015**, *253*, 65−76.
(72) Neugebauer, J.; Scheffler, M. Adsorbate-substrate and adsorbate-adsorbate interactions of Na and K adlayers on Al(111). *Phys. Rev. B* **1992**, *46*, 16067−16080.
(73) Martyna, G. J.; Tuckerman, M. E. A reciprocal space based method for treating long range interactions in ab initio and force-field-based calculations in clusters. *J. Chem. Phys.* **1999**, *110*, 2810−2821.
(74) Henkelman, G.; Uberuaga, B. P.; Jónsson, H. A climbing image nudged elastic band method for finding saddle points and minimum energy paths. *J. Chem. Phys.* **2000**, *113*, 9901−9904.
(75) Smidstrup, S.; Pedersen, A.; Stokbro, K.; Jónsson, H. Improved initial guess for minimum energy path calculations. *J. Chem. Phys.* **2014**, *140*, 214106.
(76) Henkelman, G.; Jónsson, H. A dimer method for finding saddle points on high dimensional potential surfaces using only first derivatives. *J. Chem. Phys.* **1999**, *111*, 7010−7022.
(77) Heyden, A.; Bell, A. T.; Keil, F. J. Efficient methods for finding transition states in chemical reactions: Comparison of improved dimer method and partitioned rational function optimization method. *J. Chem. Phys.* **2005**, *123*, 224101.
(78) Hjorth Larsen, A.; Jørgen Mortensen, J.; Blomqvist, J.; Castelli, I. E.; Christensen, R.; Dułak, M.; Friis, J.; Groves, M. N.; Hammer, B.; Hargus, C.; Hermes, E. D.; Jennings, P. C.; Bjerre Jensen, P.; Kermode, J.; Kitchin, J. R.; Leonhard Kolsbjerg, E.; Kubal, J.; Kaasbjerg, K.; Lysgaard, S.; Bergmann Maronsson, J.; Maxson, T.; Olsen, T.; Pastewka, L.; Peterson, A.; Rostgaard, C.; Schiøtz, J.; Schütt, O.; Strange, M.; Thygesen, K. S.; Vegge, T.; Vilhelmsen, L.; Walter, M.; Zeng, Z.; Jacobsen, K. W. The atomic simulation environment—A python library for working with atoms. *J. Phys.: Condens. Matter* **2017**, *29*, 273002.
(79) Dudarev, S. L.; Botton, G. A.; Savrasov, S. Y.; Humphreys, C. J.; Sutton, A. P. Electron-energy-loss spectra and the structural stability of nickel oxide: An LSDA+U study. *Phys. Rev. B* **1998**, *57*, 1505−1509.
(80) Loschen, C.; Carrasco, J.; Neyman, K. M.; Illas, F. First-principles LDA+U and GGA+U study of cerium oxides: Dependence on the effective U parameter. *Phys. Rev. B* **2007**, *75*, 035115.
(81) Da Silva, J. L. F.; Ganduglia-Pirovano, M. V.; Sauer, J.; Bayer, V.; Kresse, G. Hybrid functionals applied to rare-earth oxides: The example of ceria. *Phys. Rev. B* **2007**, *75*, 045121.
(82) Huang, M.; Fabris, S. CO adsorption and oxidation on ceria surfaces from DFT+U calculations. *J. Phys. Chem. C* **2008**, *112*, 8643−8648.
(83) Calaza, F. C.; Xu, Y.; Mullins, D. R.; Overbury, S. H. Oxygen vacancy-assisted coupling and enolization of acetaldehyde on CeO_2(111). *J. Am. Chem. Soc.* **2012**, *134*, 18034−18045.
(84) Bhasker-Ranganath, S.; Rahman, M. S.; Zhao, C.; Calaza, F.; Wu, Z.; Xu, Y. Elucidating the mechanism of ambient-temperature aldol condensation of acetaldehyde on ceria. *ACS Catal.* **2021**, *11*, 8621−8634.
(85) Gerward, L.; Staun Olsen, J.; Petit, L.; Vaitheeswaran, G.; Kanchana, V.; Svane, A. Bulk modulus of CeO_2 and PrO_2—An

experimental and theoretical study. *J. Alloys Compd.* **2005**, *400*, 56−61.
(86) Gerward, L.; Olsen, J. S. Powder diffraction analysis of cerium dioxide at high pressure. *Powder Diffr.* **1993**, *8*, 127−129.
(87) Mathew, K.; Sundararaman, R.; Letchworth-Weaver, K.; Arias, T. A.; Hennig, R. G. Implicit solvation model for density-functional study of nanocrystal surfaces and reaction pathways. *J. Chem. Phys.* **2014**, *140*, 084106.
(88) Mathew, K.; Kolluru, V. S. C.; Mula, S.; Steinmann, S. N.; Hennig, R. G. Implicit self-consistent electrolyte model in plane-wave density-functional theory. *J. Chem. Phys.* **2019**, *151*, 234101.
(89) Andreussi, O.; Dabo, I.; Marzari, N. Revised self-consistent continuum solvation in electronic-structure calculations. *J. Chem. Phys.* **2012**, *136*, 064102.
(90) Andreussi, O.; Marzari, N. Electrostatics of solvated systems in periodic boundary conditions. *Phys. Rev. B* **2014**, *90*, 245101.
(91) Suh, J. Model studies of metalloenzymes involving metal ions as Lewis acid catalysts. *Acc. Chem. Res.* **1992**, *25*, 273−279.
(92) Kamat, S. S.; Bagaria, A.; Kumaran, D.; Holmes-Hampton, G. P.; Fan, H.; Sali, A.; Sauder, J. M.; Burley, S. K.; Lindahl, P. A.; Swaminathan, S.; Raushel, F. M. Catalytic mechanism and three-dimensional structure of adenine deaminase. *Biochemistry* **2011**, *50*, 1917−1927.
(93) Puértolas, B.; Rellán-Piñeiro, M.; Núñez-Rico, J. L.; Amrute, A. P.; Vidal-Ferran, A.; López, N.; Pérez-Ramírez, J.; Wershofen, S. Mechanistic insights into the ceria-catalyzed synthesis of carbamates as polyurethane precursors. *ACS Catal.* **2019**, *9*, 7708−7720.
(94) Zhao, C.; Xu, Y. Theoretical investigation of dephosphorylation of phosphate monoesters on CeO_2(111). *Catal. Today* **2018**, *312*, 141−148.
(95) Bhasker-Ranganath, S.; Zhao, C.; Xu, Y. Theoretical analysis of the adsorption of phosphoric acid and model phosphate monoesters on CeO_2(111). *Surf. Sci.* **2021**, *705*, 121776.
(96) Capdevila-Cortada, M.; Vilé, G.; Teschner, D.; Pérez-Ramírez, J.; López, N. Reactivity descriptors for ceria in catalysis. *Appl. Catal. B: Environ.* **2016**, *197*, 299−312.
(97) Zaki, M. I.; Hasan, M. A.; Pasupulety, L. Surface reactions of acetone on Al_2O_3, TiO_2, ZrO_2, and CeO_2: IR spectroscopic assessment of impacts of the surface acid−base properties. *Langmuir* **2001**, *17*, 768−774.
(98) Snell, R. W.; Shanks, B. H. Insights into the ceria-catalyzed ketonization reaction for biofuels applications. *ACS Catal.* **2013**, *3*, 783−789.
(99) Xu, L.; Xu, Y. Effect of Pd surface structure on the activation of methyl acetate. *Catal. Today* **2011**, *165*, 96−105.
(100) Schneider, W. F.; Hass, K. C.; Miletic, M.; Gland, J. L. Dramatic cooperative effects in adsorption of NO_x on MgO(001). *J. Phys. Chem. B* **2002**, *106*, 7405−7413.
(101) Van den Bossche, M.; Grönbeck, H. Adsorbate pairing on oxide surfaces: Influence on reactivity and dependence on oxide, adsorbate pair, and density functional. *J. Phys. Chem. C* **2017**, *121*, 8390−8398.
(102) Castelli, I. E.; Man, I.-C.; Soriga, S.-G.; Parvulescu, V.; Halck, N. B.; Rossmeisl, J. Role of the band gap for the interaction energy of coadsorbed fragments. *J. Phys. Chem. C* **2017**, *121*, 18608−18614.
(103) Fernández-Torre, D.; Kośmider, K.; Carrasco, J.; Ganduglia-Pirovano, M. V.; Pérez, R. Insight into the adsorption of water on the clean CeO_2(111) surface with van der Waals and hybrid density functionals. *J. Phys. Chem. C* **2012**, *116*, 13584−13593.
(104) Molinari, M.; Parker, S. C.; Sayle, D. C.; Islam, M. S. Water adsorption and its effect on the stability of low index stoichiometric and reduced surfaces of ceria. *J. Phys. Chem. C* **2012**, *116*, 7073−7082.
(105) Ren, Z.; Liu, N.; Chen, B.; Li, J.; Mei, D. Theoretical investigation of the structural stabilities of ceria surfaces and supported metal nanocluster in vapor and aqueous phases. *J. Phys. Chem. C* **2018**, *122*, 4828−4840.
(106) Florián, J.; Warshel, A. Langevin dipoles model for ab initio calculations of chemical processes in solution: Parametrization and application to hydration free energies of neutral and ionic solutes and conformational analysis in aqueous solution. *J. Phys. Chem. B* **1997**, *101*, 5583−5595.
(107) Florián, J.; Warshel, A. Calculations of hydration entropies of hydrophobic, polar, and ionic solutes in the framework of the langevin dipoles solvation model. *J. Phys. Chem. B* **1999**, *103*, 10282−10288.
(108) Beicastro, M.; Marino, T.; Mineva, T.; Russo, N.; Sicilia, E.; Toscano, M. Density functional theory as a tool for the prediction of the properties in molecules with biological and pharmacological significance. *Theor. Comput. Chem.* **1996**, *4*, 743−772.
(109) Nørskov, J. K.; Bligaard, T.; Logadottir, A.; Bahn, S.; Hansen, L. B.; Bollinger, M.; Bengaard, H.; Hammer, B.; Sljivancanin, Z.; Mavrikakis, M.; Xu, Y.; Dahl, S.; Jacobsen, C. J. H. Universality in heterogeneous catalysis. *J. Catal.* **2002**, *209*, 275−278.
(110) Abild-Pedersen, F.; Greeley, J.; Studt, F.; Rossmeisl, J.; Munter, T. R.; Moses, P. G.; Skúlason, E.; Bligaard, T.; Nørskov, J. K. Scaling properties of adsorption energies for hydrogen-containing molecules on transition-metal surfaces. *Phys. Rev. Lett.* **2007**, *99*, 016105.
(111) Li, T.; Tsyshevsky, R.; Algrim, L.; McEntee, M.; Durke, E. M.; Eichhorn, B.; Karwacki, C.; Zachariah, M. R.; Kuklja, M. M.; Rodriguez, E. E. Understanding dimethyl methylphosphonate adsorption and decomposition on mesoporous CeO_2. *ACS Appl. Mater. Interfaces* **2021**, *13*, 54597−54609.
(112) Beste, A.; Overbury, S. H. Methyl formate formation during methanol conversion over the (111) ceria surface. *J. Phys. Chem. C* **2017**, *121*, 9920−9928.

https://doi.org/10.1021/acscatal.2c02514
ACS Catal. 2022, 12, 10222−10234